

Article

Sensor-Embedded Face Masks for Detection of Volatiles in Breath: A Proof of Concept Study

Lorena Di Zazzo ¹, Gabriele Magna ², Martina Lucentini ¹, Manuela Stefanelli ², Roberto Paolesse ²
and Corrado Di Natale ^{1,*}

¹ Department of Electronic Engineering, University of Rome Tor Vergata, via del Politecnico 1, 00133 Rome, Italy; dizazzo_94@libero.it (L.D.Z.); martina.lucentini.1995@gmail.com (M.L.)

² Department of Chemical Science and Technology, University of Rome Tor Vergata, via della Ricerca Scientifica, 00133 Rome, Italy; gabriele.magna@uniroma2.it (G.M.); manuela.stefanelli@uniroma2.it (M.S.); paolesse@uniroma2.it (R.P.)

* Correspondence: dinatale@uniroma2.it

Abstract: The correlation between breath volatiles and health is prompting a growing interest in the development of sensors optimized for breath analysis. On the other hand, the outbreak of COVID-19 evidenced that breath is a vehicle of infection; thus, the introduction of low-cost and disposable devices is becoming urgent for a clinical implementation of breath analysis. In this paper, a proof of concept about the functionalization of face masks is provided. Porphyrin-based sensors are among the most performant devices for breath analysis, but since porphyrins are scarcely conductive, they make use of costly and bulky mass or optical transducers. To overcome this drawback, we introduce here a hybrid material made of conducting polymer and porphyrins. The resulting material can be easily deposited on the internal surface of standard FFP face masks producing resistive sensors that retain the chemical sensitivity of porphyrins implementing their combinatorial selectivity for the identification of volatile compounds and the classification of complex samples. The sensitivity of sensors has been tested with respect to a set of seven volatile compounds representative of diverse chemical families. Sensors react to all compounds but with a different sensitivity pattern. Functionalized face masks have been tested in a proof-of-concept test aimed at identifying changes of breath due to the ingestion of beverages (coffee and wine) and solid food (banana- and mint-flavored candies). Results indicate that sensors can detect volatile compounds against the background of normal breath VOCs, suggesting the possibility to embed sensors in face masks for extensive breath analysis

Keywords: breath analysis; face mask; gas sensors; porphyrins; PEDOT:PSS



Citation: Di Zazzo, L.; Magna, G.; Lucentini, M.; Stefanelli, M.; Paolesse, R.; Di Natale, C. Sensor-Embedded Face Masks for Detection of Volatiles in Breath: A Proof of Concept Study. *Chemosensors* **2021**, *9*, 356. <https://doi.org/10.3390/chemosensors9120356>

Academic Editor: Takahiro Arakawa

Received: 4 November 2021

Accepted: 9 December 2021

Published: 12 December 2021

Publisher's Note: MDPI stays neutral with regard to jurisdictional claims in published maps and institutional affiliations.



Copyright: © 2021 by the authors. Licensee MDPI, Basel, Switzerland. This article is an open access article distributed under the terms and conditions of the Creative Commons Attribution (CC BY) license (<https://creativecommons.org/licenses/by/4.0/>).

1. Introduction

The composition of human metabolome depends on natural life events such as the menstrual cycle [1] and circadian rhythms [2] and by pathophysiological events [3].

The fraction of metabolome made of volatile or semi-volatile compounds, the volatiles, has been the subject of extensive studies [4]. In particular, evidence about the diagnostic and prognostic properties of volatiles released by various human compartments has been shown [5]. About 34% of the human volatiles is found in breath [6]; thus, also thanks to the high accessibility of the sample, breath analysis has been widely investigated in order to correlate its composition with different life processes including those characteristics of pathologies and conditions [7].

The volatile compounds in breath originate in various organs and tissues; they are collected by blood and transferred to breath at the blood/air interface in the lungs [8]. The migration from blood to breath depends on the physical characteristics of the molecules and on their partition coefficient at the respective interfaces. For instance, non-water-soluble

hydrocarbons are more abundant in breath than in urine, while ketones are more likely found in urines than in breath [6].

Breath analysis has been mostly based on collecting breath in sterile bags or in an adsorbant substrates. The sterile bag approach seems the most effective, and it has been used to study the relationship between breath volatilome and lung cancer [9]. However, the collection of breath samples may be subject to several drawbacks, not least their contamination by pathogens. Breath is the preferential way of transmission of bacteria and viruses. Virus filters enables the collection of breath in sterile bags, as shown by a study about tuberculosis [10]. The outbreak of SARS-COV-2 shown that the infection can be spread by both asymptomatic and pre-symptomatic individuals [11]; thus, in the event of a pandemic virus, the filters should be included in any breath sampler.

A viable alternative to a breath sampler is the use of sensors embedded in face masks [12]. Masks are mainly made of cellulose, a material that has been investigated as a substrate for wearable and paper-based sensors [13,14]. Besides being used as substrate for sensors, cellulose can also act as a sensitive layer for humidity [15,16]; indeed, the adsorption of water molecules in cellulose layer increases the conductivity, which can be easily measured by printed electrodes. This mechanism was applied to develop respiration rate sensors. Furthermore, adsorbed water can also offer the chance to detect water soluble gases, since these species may dissociate in the moisture, giving rise to ionic charges that increases the conductivity of the cellulose layer. This method has been demonstrated to be effective for the detection of ammonia [17].

In this paper, this concept has been further extended, introducing on top of the cellulose a water-soluble organic film. In practice, the presence of the molecular film is expected to further interact with hydrophilic molecules, differentiating the response according to the affinity with the organic layer. For the scope, four different hybrid materials made of mixtures of porphyrins and a conductive polymer were utilized.

Porphyrin-based gas sensors have been used in several volatilome applications, for instance, to diagnose lung cancer from breath [18] and COVID-19 from serum [19]. Porphyrins are barely conductive; thus, they are mostly used with optical or mass transducers. Here, resistive sensors are obtained mixing porphyrins with PEDOT:PSS polymer composite (poly(3,4-ethylenedioxythiophene):polystyrene sulfonate). PEDOT:PSS is a conductive polymer largely used in organic electronics [20] as a chemical sensor [21].

Porphyrins and PEDOT:PSS are both biocompatible. For instance, PEDOT:PSS is used to contact human skin for biomedical applications [22], while porphyrins, besides their biological origin, are utilized for in vivo photodynamic therapy [23].

The change in resistance of sensors deposited onto face masks has been measured in the presence of a series of volatile compounds representative of different chemical families. As expected, sensors are not individually selective, but their ensemble can univocally identify chemical compounds and mixtures implementing the combinatorial selectivity principle [24].

To test the sensors for breath analysis, they have been deposited on the internal surface of commercially available FFP2 face masks. The sensors have been tested to discriminate breath collected after the uptake of different foods. Results show that even a little sensor array made of only three sensors is enough to discriminate between the different foods, namely, it can distinguish the addition of compounds to human breath volatilome. These results illustrate the feasibility of the chemical functionalization of face masks in order to develop low-cost disposable sensor arrays for breath analysis.

2. Materials and Methods

The sensitive material was designed as a hybrid between a conductive polymer and a chemically sensitive molecule. Two water-soluble porphyrins were chosen for the scope: 5,10,15,20-tetrakis-(4-sulfonatophenyl) porphyrin (hereafter, TPPS) and (N-methyl-4-pyridyl)porphyrin (hereafter, TPyP). Both molecules were used as a free base (H_2 TPPS and H_2 TPyP) and manganese complex (MnTPPS and MnTPyP). The manganese complexes

also contain a chlorine atom as counterion. The chemical structure of the four porphyrins is shown in Figure 1.

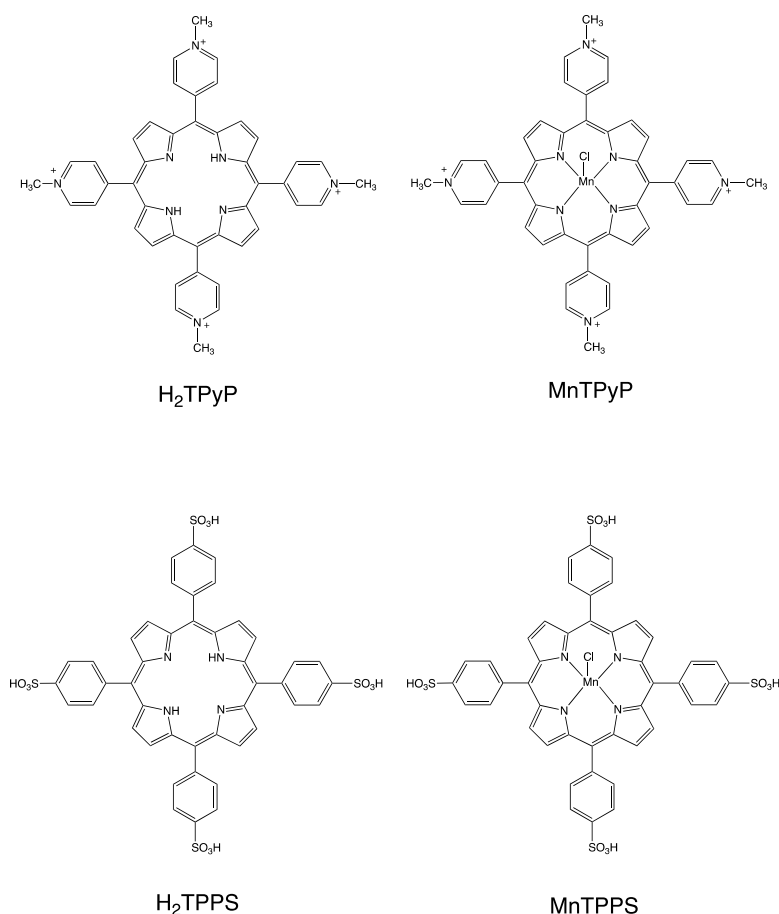


Figure 1. Molecular structure of the four studied porphyrins.

The sensing properties of these porphyrins were studied in the past. TPPS was used to prepare nanostructured sensors [25] and to functionalize ZnO nanostructures [26], while TPyP was used to functionalize graphene oxide sheets [27].

Commercial PEDOT:PSS (Clevios PH500, 1.3 wt% in water) 1:2.5 was firstly diluted in water (1:10 *v/v*) and then mixed with a proper aliquot of aqueous solution of porphyrin (1 μ M) to obtain porphyrin-polymer 1/1 wt. To facilitate the deposition on face masks, a small amount of ethanol, 1:10 *v/v*, was added to the solution. The presence of ethanol reduces the contact angle between the solution droplets and the surface of the face mask, favoring the formation of a compact film.

Porphyrins and PEDOT:PSS solutions were spotted onto the internal surface of FFP2 face masks. The deposition protocol consisted of depositing 20 μ L of hybrid solutions onto the internal surface of the mask and left to evaporate overnight under standard laboratory conditions (20–25 °C with humidity levels between 30% and 50%). The drop-casting procedure was repeated three times to produce a compact film, moderately conductive with no cracks or macroscopic inhomogeneities. Masks, purchased in a local shop, were duly certified for human use according to the European Union rules. UV–Vis spectra have been carried out with Agilent Cary 100 spectrophotometer, and micrographic characterization using a field emission scanning electron microscope (FE-SEM, SUPRA™ 35, Carl Zeiss SMT, Oberkochen, Germany).

To measure the electric resistance, each spot was contacted with electrodes made of a conductive graphite paste.

In order to characterize the sensor responses, pieces of functionalized FFP2 masks were accommodated in a sealed chamber. The electric resistance has been measured with a digital multimeter endowed with a multiplexed input ($7\frac{1}{2}$ -digit model 2001, Keithley). The resistances of sensors in a flux of synthetic air are shown in Table 1. These values correspond to the baseline of sensor responses to gases. It is interesting to observe that a noticeable difference in sensor conductivity results from films containing the different porphyrins utilized. In particular, free base porphyrins are more conductive than their metal complexes.

Table 1. Baseline resistance of prepared sensors.

Sensor	Resistance
PEDOT:PSS	38 k Ω
PEDOT:PSS + H ₂ TPPS	315 k Ω
PEDOT:PSS + MnTPPS	1 M Ω
PEDOT:PSS + H ₂ TPyP	114 k Ω
PEDOT:PSS + MnTPyP	850 M Ω

Sensors were exposed to vapors of ethanol, water, hexane, toluene, acetone, acetic acid, and triethylamine. These compounds were chosen as representative of different chemical families. High-grade purity compounds were purchased from Sigma Aldrich and used without further purification. Double-distilled water was used to test humidity responses. For each compound, measurements were carried out exposing the sensors to different concentrations obtained mixing the saturated vapors of liquid compounds with a stream of nitrogen gas. A pure stream of nitrogen gas was used to restore the sensor response and to define the sensors baseline. Since saturated vapor pressure depends on temperature, the liquid compounds were kept at 20 °C in a thermal bath. Saturated vapor pressures were calculated with Antoine's equation, using the parameters available at the NIST database (<https://webbook.nist.gov/chemistry/> accessed on 10 December 2021). Measurements were performed at 20 °C.

Sensor data were analyzed in Matlab (R_2020b) and using the Statistics and Machine Learning Toolbox (version 11.7).

3. Results

The interaction between PEDOT:PSS and porphyrins was studied measuring the optical absorption spectra in water (see Figure 2). The PEDOT:PSS spectrum (data not shown) is characterized by a broaden peak centered in the near IR region (800 nm) due to the extended conjugated system responsible for conductivity. The negligible absorbance for wavelengths up to 550 nm allows the clear emergence of the Soret bands.

The spectra of porphyrins mixed with PEDOT:PSS do not show band broadenings, indicating the absence of aggregation and a good molecular dispersion in the polymer matrix. The Soret band of the porphyrin free bases experiences a red shift, probably induced by the electrostatic interaction with the charged polymer. A different behavior is observed for the Mn complexes, where a blue shift is present, also with a variation of the relative intensity of the metal-to-ligand charge transfer band. Both of these features indicate a variation of the coordinative behavior of the Mn ion upon interaction with the polymer matrix. These porphyrin–polymer interactions may result in the capability of porphyrins to interfere or modulate the conductivity properties of PEDOT:PSS once spotted on solid films. This mechanism is at the basis of developing improved chemical-active materials based on conductive polymers combined with porphyrins [28]. The different interactions between porphyrins and PEDOT:PSS is a fundamental feature of these sensors, because it suggests the possibility to develop sensor arrays.

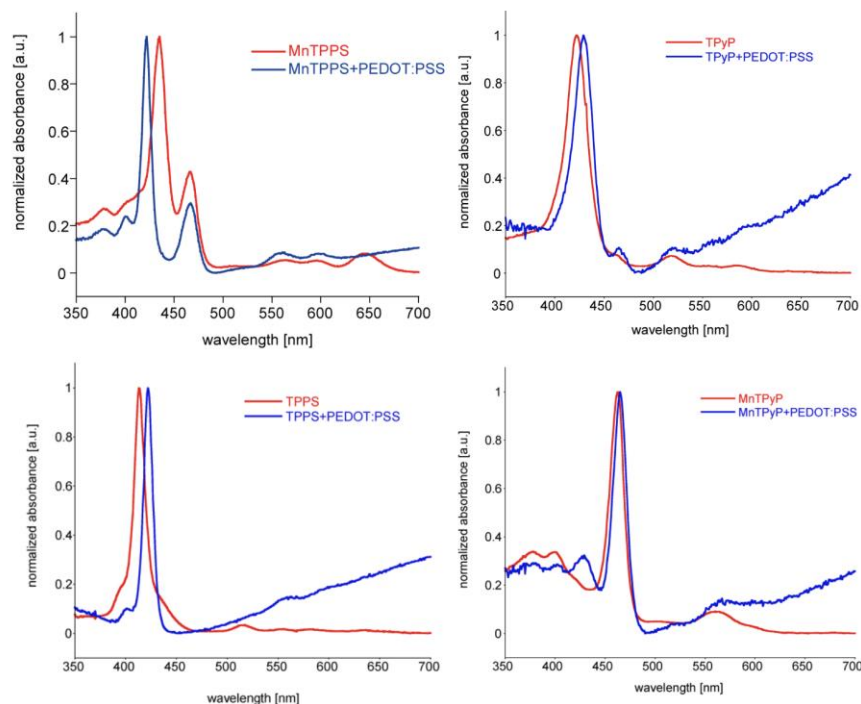


Figure 2. Absorption spectra of porphyrins and porphyrins–PEDOT:PSS mixture in water.

Figure 3 shows the SEM images of films produced by spotting porphyrins–PEDOT:PSS mixtures onto the FFP2 face mask. The polymer forms a continuous layer, porphyrins are homogeneously dissolved in the polymeric matrix, and neither molecular aggregation nor clusters are visible in these images.

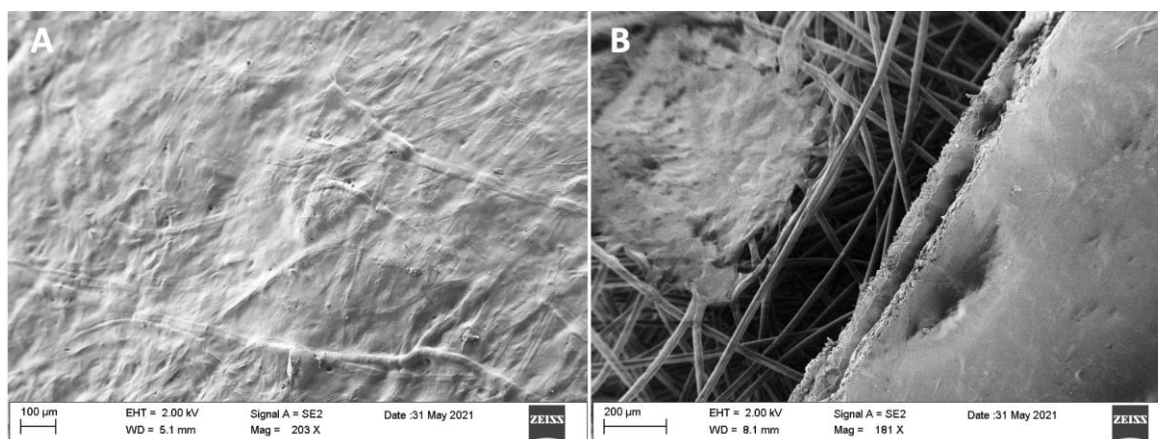


Figure 3. SEM image of PEDOT:PSS + H₂TPyP on the internal surface of FFP2 face mask. (A) polymer–molecular mixture is homogeneously distributed onto the surface, and the underlying cellulose fibers are visible. (B) a lateral view of a cracked film shows the compact layered arrangement of the sensitive film. The stratifications of layers correspond to successive steps of deposition.

The gas sensitivity was measured exposing the sensors to various concentrations of the volatile compounds. The sensor response was evaluated as the relative change of the resistance measured during the exposure to vapors with respect to the resistance measured immediately before the exposure. Along with hybrid porphyrin–PEDOT:PSS materials, pristine PEDOT:PSS was tested as reference. Figure 4 shows the response curve of the five sensors to the tested gases. The response curve is almost linear, and sensors show a different response to the various gases. The concentration of VOCs has been estimated with

Antoine's equation, and it has not been further validated by independent measurements. However, the almost linear response of the sensors respect to the concentration shows that at least in terms of changes of concentration the estimates are sufficiently correct. It is interesting to note that, compared to the bare PEDOT:PSS sensor, the presence of porphyrins increases the response to acetone and non-water-soluble VOCs (toluene and hexane). Surprisingly, the sensors show a non-negligible response to hexane, for which the supposed sensing mechanism is not expected to be valid. The sensitivity to hexane is likely due only to the polymer swelling consequent to the molecular absorption [29].

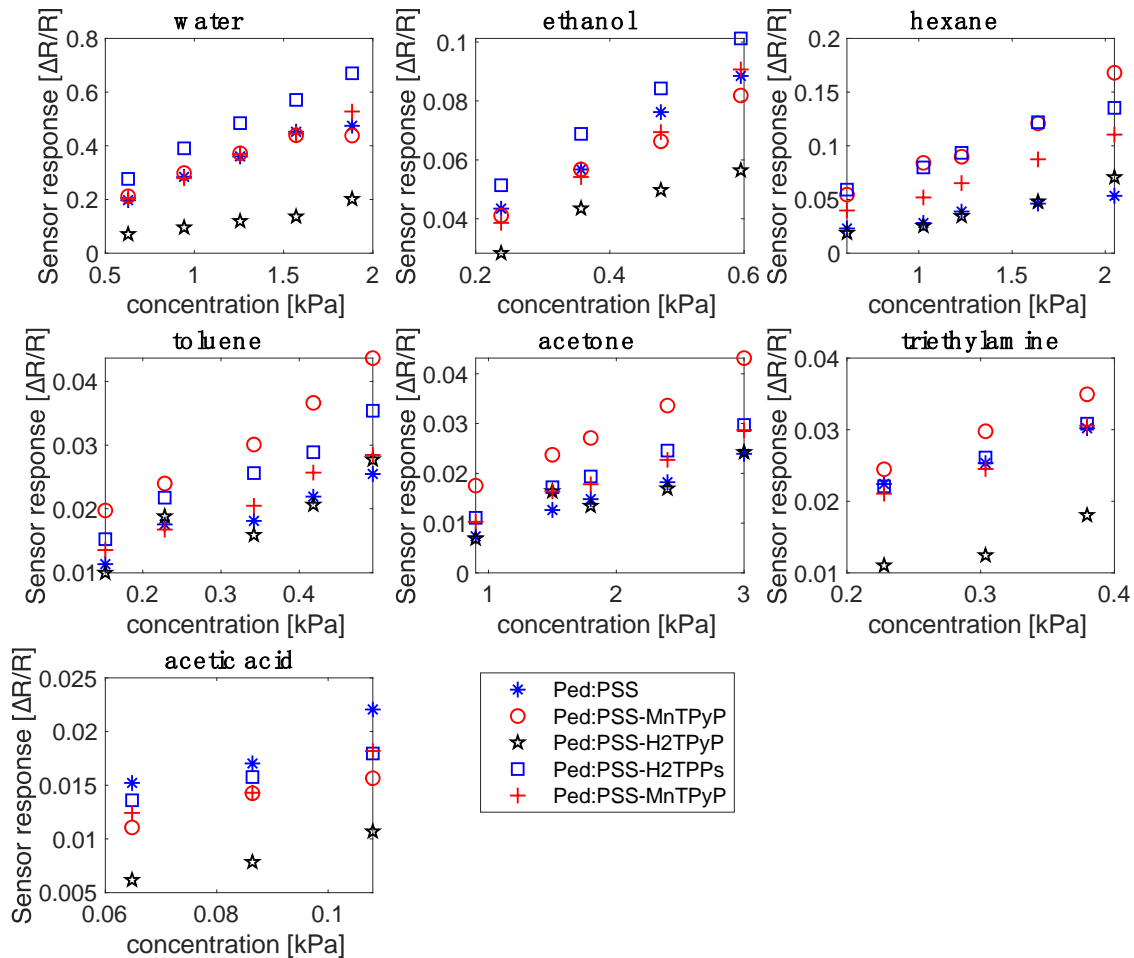


Figure 4. Response curves to the seven studied volatile compounds.

The largest response is achieved for water vapor; this is expected, considering that water is the solvent utilized to disperse the PEDOT:PSS polymer. However, it is important also to take into account that, as a result of the diverse saturation pressure, the ranges of concentration are different. Hexane and acetone, being the most volatile of the tested compounds, have been measured at the largest concentration. Water was tested in an extended range (20–60%) due to the large content usually found in both environmental air and human breath.

To better appraise the sensor response, it is convenient to compare the sensitivity of the sensors, namely, the slope of the linear fit of response curves (see Figure 5) [30]. The concentration of VOCs for sensor calibration was obtained by diluting the saturated vapor pressures with a nitrogen flux. The dilution factor is limited by the mass flow controllers, and it was settled between 3 and 10%. On the other hand, the calculated sensitivities enable to extrapolate the sensor response at smaller concentrations. For instance, the sensitivity to ethanol PEDOT:PSS + H₂TTPS is about 0.13 kPa⁻¹ (see Figure 5). At the partial pressure of

1 Pa, the expected relative change of resistance is $\Delta R/R = 0.13 \times 10^{-3}$. Considering that the baseline resistance of the sensor is 315 K Ω (Table 1), the estimated change of resistance is about 44 Ω , a value detectable with the used digital multimeter.

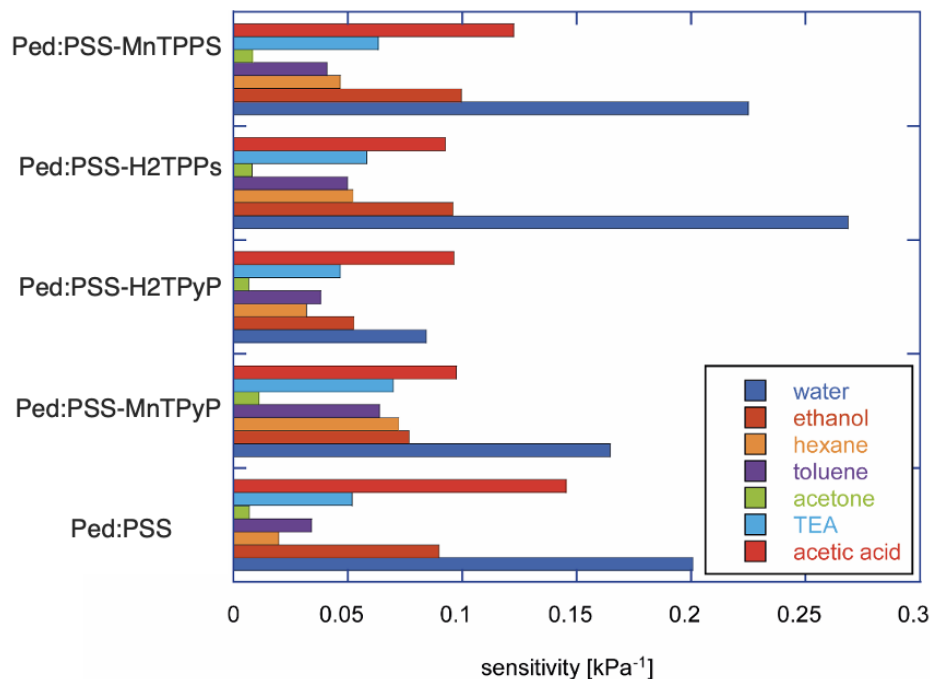


Figure 5. Sensitivity of sensors to the seven tested compounds.

The large sensitivity to water of TPPS was known from previous studies [31]. However, porphyrins sensors show a rather different pattern of sensitivities respect to the pristine PEDOT:PSS. Interestingly, in the case of TPyP, the sensitivity to water is reduced in favor of other compounds that are sensed relatively higher. The different patterns of sensitivities indicate that these sensors are suitable to implement the combinatorial selectivity, and thus, they might be used as an electronic nose to identify volatile compounds either pure or in complex mixtures.

A demonstration of this possibility is achieved by analyzing the sensor data in Figure 4 with the principal component analysis (PCA). Since variable concentration is a confounding factor, the data have been linearly normalized to reduce the effect of concentration [32]. The normalization consists of dividing the response of each sensor to the norm of the multivariate sensor response, according to the following transformation:

$$\left(\frac{\Delta R}{R}\right)_{ij}^* = \frac{\left(\frac{\Delta R}{R}\right)_{ij}}{\sqrt{\sum_k \left(\frac{\Delta R}{R}\right)_{ij}^2}}, \quad (1)$$

where $(\Delta R/R)_{ij}$ is the response of the i th sensor to the j th compound, and the summation is extended to all the sensors of the array.

In the case of perfect linearity between sensor response and concentration, the above transformation gives rise to a novel response, which is independent from the concentration, and it only contains the sensitivity of the sensor divided by the sum of the sensitivities of all sensors of the array. The independence of the transformed response from the concentration enables the appraisal of the sensor response without considering the particular tested range of concentration. Furthermore, it evaluates the performance of each sensor compared to the other sensors of the array.

The results of the PCA of transformed responses are shown in Figure 6. Figure 6A shows the plot of the first two principal components, where about 91% of the

total variance of the data set is explained. The data related to each compound form close clusters. Compounds are arranged in groups that are related to the kind of interaction between sensors and volatile compounds. Hexane and water are largely separated from the other compounds. This suggests a great difference of interaction between these compounds and the sensors. Indeed, hexane is expected to establish dispersion interactions with the organic materials, while in water, hydrogen bonds are dominant. In other cases, a mixture of interactions including electron–donor and π – π interactions take place. The loadings plot in Figure 6B shows the relationship between volatile compounds and sensors. PEDOT:PSS in mixture with MnTPPS is characterized by the smallest loadings, and it provides a little contribution to the array. The mutual orthogonal direction of PEDOT:PSS and its mixtures with Mn-TPyP, H₂TPPS, and H₂TPyP form a reference base for the compounds representation in Figure 6A, and it shows good complementarity of the five sensors.

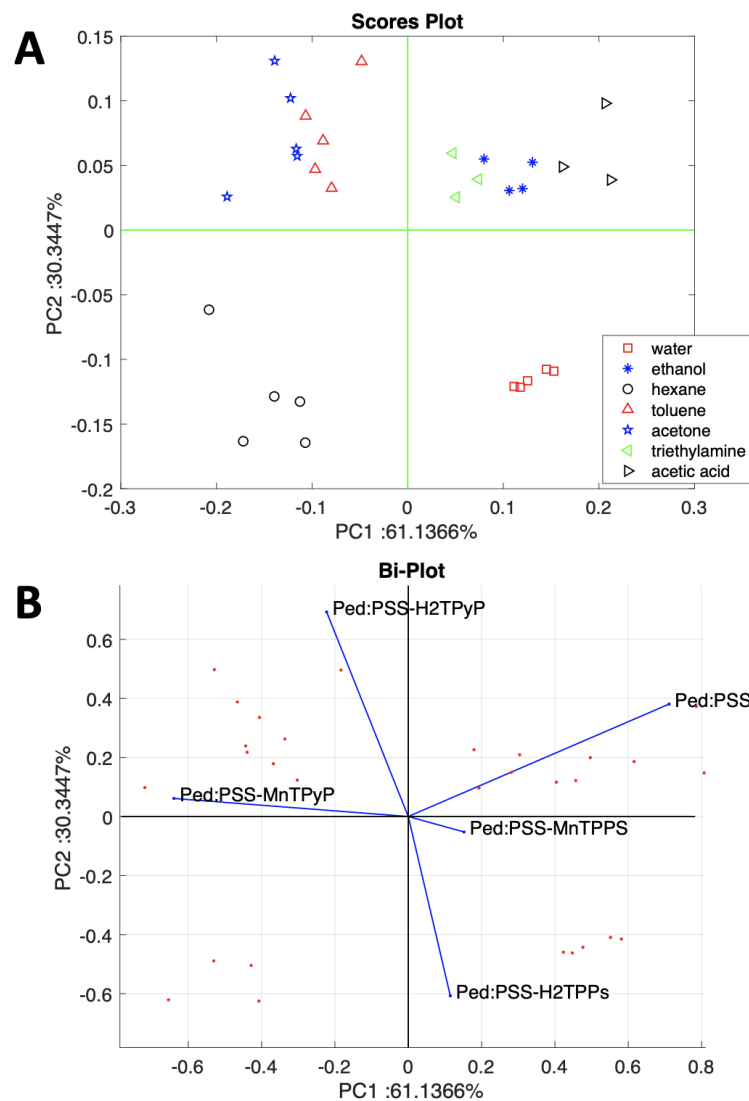


Figure 6. PCA of volatile compounds data. (A) scores plot of the first two principal components. (B) corresponding loadings plot.

A breath test was performed by depositing three sensors on the internal surface of face masks. Based on the loading plot in Figure 6B, the chosen sensors were PEDOT:PSS, PEDOT:PSS + H₂TPyP, and PEDOT:PSS + MnTPyP. These sensors are sufficiently orthogonal in the scores plot plane and ensure a good coverage of the tested compounds. Figure 7A shows a detail of the sensors on the internal surface of the mask. The sensor

occupies less than 2% of the internal area of the mask, and this amount cannot significantly reduce the total filtration of the mask. Here, the measurement protocol required short use of the mask. Sensors were tested by four volunteers. During the measurement, each person was asked to perform two cycles of respiration at low and normal frequency [33].

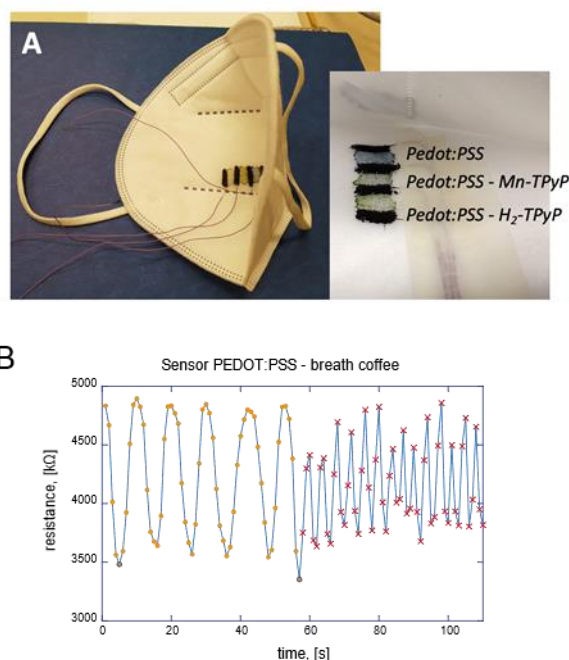


Figure 7. (A) Detail of the sensors deposited on the internal surface of the face mask. (B) Signal of PEDOT:PSS sensor taken after coffee ingestion. The measurement consists of two sequences of respirations at slow and normal rates (about 6 and 14 breaths per minute).

A test has been performed to study the capability of the sensors to discriminate breaths after the ingestion of different foods. The analyzed food stuffs were a mint pastil, 50 g of banana, 20 mL of espresso coffee, and 10 mL of red wine.

Before each ingestion, the subjects rinsed their mouths with water and wore a functionalized face mask one minute after the ingestion of a foodstuff. The subject freely breathed for one minute and then performed two sequences of respiration at the rate of 6 and 14 breaths per minute. After each measurement, the subject waited one hour before testing another food. For each subject, the foods sequence was randomized. Measurements took place in the afternoon, 2 h after the last meal. Except water, no other beverage was consumed between the meal and the measurement session.

Figure 7B shows the sequence of measurement of one subject after coffee ingestion.

Due to the sensitivity to humidity, the sensor signal follows the respiration rate. However, even other compounds in breath are modulated by the respiration. Thus, considering the results in Figure 6, we may expect that the sensors can detect the differences between foods.

From the sequence of measurements in Figure 7B, two features have been calculated for low and normal respiration rates, respectively. The features correspond to the average difference of maximum and minimum resistance in each respiratory cycle. Figure 8 shows the distribution of sensor responses of the four subjects taken at low (Figure 8A) and normal (Figure 8B) frequency rates.

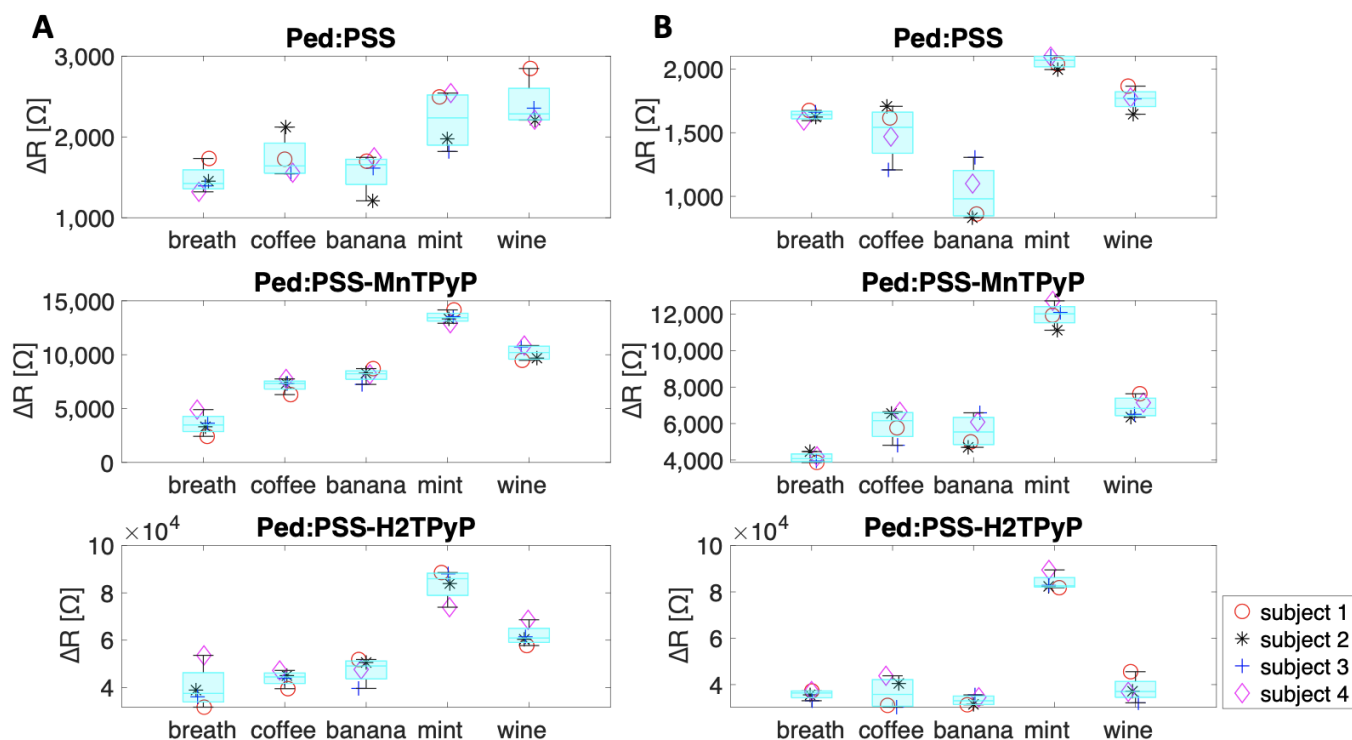


Figure 8. Distribution of the responses of sensors to the basic breath and the ingested foods. (A) low frequency breath, (B) normal frequency breath. The response of each subject is indicated by a different marker. The class labelled as breath indicates the basic breath before the ingestion of food.

Data show that, independently of the modality of breath, porphyrin sensors have a strong response to mint, but the separation between foods is more evident in the low-frequency breath rate modality. In the case of PEDOT:PSS, normal frequency data show a better recognition of mint.

Normal breath rate and slow breath rate features have been separately analyzed with PCA. Results are shown in Figure 9.

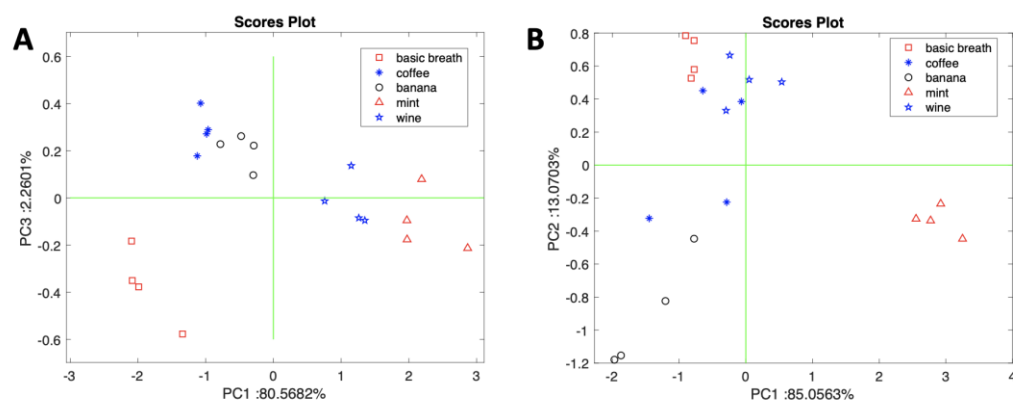


Figure 9. PCA scores plot of features calculated on the slow breath rate signal (A) and normal breath rate signals (B).

Figure 9A shows the scores plot in the plane of the first two principal components calculated with the features extracted from the low frequency respiration rate portion of the signal. The first two principal components explain about 83% of the total variance. Background breath samples collected before measurements are clearly separated from the samples taken after food intake. Foods form close clusters clearly separated each other.

In Figure 9B, the PCA of normal breath rate data is shown. In this case, the total variance in the scores plot is 98%, indicating a large correlation among the sensors that cannot account for the specific differences between the foods. The difference between background breath and foods is partially lost, and only mint forms a clearly separated cluster. As shown in Figure 7B, the signal during normal breath rate is characterized by a reduced number of samples per cycle. Thus, the reduced capability to identify foods with normal breath rate may be also a consequence of the fact that the evaluation of average differences between the maximum and minimum signal are more uncertain and fluctuating respect to the slow breath rate.

4. Discussion

The results described in the previous section support the concept that sensors can be implemented on the cellulose surface of face masks in order to prepare low-cost disposable devices for breath analysis. An original sensor material has been prepared, combining together the conductive properties of PEDOT:PSS with the chemical sensitivity of porphyrins. Two different porphyrins have been considered (TPyP and TPPS), each as a free base and manganese complex. The response of sensors (see Figures 4 and 5) shows that the hybrid materials behave as a chemoresistance, and the sensitivity is largely determined by the properties of porphyrins. As usual for porphyrin-based sensors, the devices are sensitive but scarcely selective. However, the sensitivity patterns (see Figure 5) are sufficiently different to implement the combinatorial selectivity principle, so that, even if each individual sensor is non-selective, the whole sensor array, as shown by the PCA scores plot (see Figure 6), identifies pure compounds belonging to a variety of chemical families.

Porphyrins labeled as TPyP show a better cooperation in the array, as evidenced in the loadings plot in Figure 6B, where these porphyrins are those that contribute most to the detection of volatile compounds and those that contribute less with respect to water. As a consequence, these porphyrins have been chosen to be implemented in a face mask in order to be tested as sensors for breath analysis. The coarseness of the deposition method and the limited available space inside the mask restricted number of sensors to three.

Functionalized face masks were tested in a simple experiment aimed at identifying changes in breath composition after the ingestion of various foodstuffs. Sensors are very sensitive to humidity, so the sensor signals follow the rate of breath. This characteristic has been used to determine a sensor feature defined as the average difference between the maximum and minimum signal achieved in a sequenced of breath. In spite of the water content and the high water concentration in breath, the sensors are shown to be sensitive with respect to specific food-related compounds. Slow and normal breath rates have been considered, and results show that the signals obtained during a sequence of slow breaths can easily identify the foodstuff.

5. Conclusions

In this paper, a proof of concept of face masks functionalized with chemical sensors has been provided. The low-cost and simplicity of preparation of these sensors allows for the use of these devices for breath analysis. The final scope is to replicate the results achieved by porphyrin sensors in breath analysis with disposable and safe sensor systems.

Author Contributions: Conceptualization: C.D.N., R.P. and G.M.; methodology: G.M. and C.D.N.; investigation: L.D.Z., G.M., M.S. and M.L.; writing—original draft preparation: C.D.N. All authors have read and agreed to the published version of the manuscript.

Funding: This research received no external funding.

Informed Consent Statement: Informed consent was obtained from all subjects involved in the study.

Conflicts of Interest: The authors declare no conflict of interest.

References

1. Eshima, J.; Ong, S.; Davis, T.J.; Miranda, C.; Krishnamurthy, D.; Nachtsheim, A.; Stufken, J.; Plaisier, C.; Fricks, J.; Bean, H.D.; et al. Monitoring changes in the healthy female metabolome across the menstrual cycle using GC × GC-TOFMS. *J. Chromatogr. B* **2019**, *1121*, 48–57. [\[CrossRef\]](#)
2. Kinouchi, K.; Mikami, Y.; Kanai, T.; Itoh, H. Circadian rhythms in the tissue-specificity from metabolism to immunity: Insights from omics studies. *Mol. Asp. Med.* **2021**, *80*, 100984. [\[CrossRef\]](#)
3. Wishart, D.S. Metabolomics for Investigating Physiological and Pathophysiological Processes. *Physiol. Rev.* **2019**, *99*, 1819–1875. [\[CrossRef\]](#)
4. Amann, A.; Costello, B.D.L.; Miekisch, W.; Schubert, J.; Buszewski, B.; Pleil, J.; Ratcliffe, N.; Risby, T. The human volatilome: Volatile organic compounds (VOCs) in exhaled breath, skin emanations, urine, feces and saliva. *J. Breath Res.* **2014**, *8*, 34001. [\[CrossRef\]](#)
5. Dummer, J.; Storer, M.; Swanney, M.; McEwan, M.; Scott-Thomas, A.; Bhandari, S.; Chambers, S.; Dweik, R.; Epton, M. Analysis of biogenic volatile organic compounds in human health and disease. *TrAC Trends Anal. Chem.* **2011**, *30*, 960–967. [\[CrossRef\]](#)
6. Drabińska, N.; Flynn, C.; Ratcliffe, N.; Belluomo, I.; Myridakis, A.; Gould, O.; Fois, M.; Smart, A.; Devine, T.; Costello, B.P.J.D.L. A literature survey of all volatiles from healthy human breath and bodily fluids: The human volatilome. *J. Breath Res.* **2021**, *15*, 34001. [\[CrossRef\]](#) [\[PubMed\]](#)
7. Beauchamp, J.; Davis, C.; Pleil, J. *Breathborne Biomarkers and the Human Volatilome*; Elsevier: Amsterdam, The Netherlands, 2020.
8. Haick, H.; Broza, Y.Y.; Mochalski, P.; Ruzsanyi, V.; Amann, A. Assessment, origin, and implementation of breath volatile cancer markers. *Chem. Soc. Rev.* **2014**, *43*, 1423–1449. [\[CrossRef\]](#)
9. Gasparri, R.; Santonico, M.; Valentini, C.; Sedda, G.; Borri, A.; Petrella, F.; Maisonneuve, P.; Pennazza, G.; D'Amico, A.; Di Natale, C.; et al. Volatile signature for the early diagnosis of lung cancer. *J. Breath Res.* **2016**, *10*, 16007. [\[CrossRef\]](#)
10. Zetola, N.M.; Modongo, C.; Matsiri, O.; Tamuhla, T.; Mbongwe, B.; Matlhagela, K.; Sepako, E.; Catini, A.; Sirugo, G.; Martinelli, E.; et al. Diagnosis of pulmonary tuberculosis and assessment of treatment response through analyses of volatile compound patterns in exhaled breath samples. *J. Infect.* **2017**, *74*, 367–376. [\[CrossRef\]](#) [\[PubMed\]](#)
11. Wiersinga, W.J.; Rhodes, A.; Cheng, A.C.; Peacock, S.J.; Prescott, H.C. Pathophysiology, Transmission, Diagnosis, and Treatment of Coronavirus Disease 2019 (COVID-19): A Review. *JAMA* **2020**, *324*, 782–793. [\[CrossRef\]](#)
12. Xue, Q.; Kan, X.; Pan, Z.; Li, Z.; Pan, W.; Zhou, F.; Duan, X. An intelligent face mask integrated with high density conductive nanowire array for directly exhaled coronavirus aerosols screening. *Biosens. Bioelectron.* **2021**, *186*, 113286. [\[CrossRef\]](#)
13. Ahmed, S.; Bui, M.-P.N.; Abbas, A. Paper-based chemical and biological sensors: Engineering aspects. *Biosens. Bioelectron.* **2016**, *77*, 249–263. [\[CrossRef\]](#) [\[PubMed\]](#)
14. Park, T.; Kim, N.; Kim, D.; Kim, S.-W.; Oh, Y.; Yoo, J.-K.; You, J.; Um, M.-K. An Organic/Inorganic Nanocomposite of Cellulose Nanofibers and ZnO Nanorods for Highly Sensitive, Reliable, Wireless, and Wearable Multifunctional Sensor Applications. *ACS Appl. Mater. Interfaces* **2019**, *11*, 48239–48248. [\[CrossRef\]](#) [\[PubMed\]](#)
15. Unander, T.; Nilsson, H.-E. Characterization of Printed Moisture Sensors in Packaging Surveillance Applications. *IEEE Sens. J.* **2009**, *9*, 922–928. [\[CrossRef\]](#)
16. Güder, F.; Ainla, A.; Redston, J.; Mosadegh, B.; Glavan, A.; Martin, T.J.; Whitesides, G.M. Paper-Based Electrical Respiration Sensor. *Angew. Chem. Int. Ed.* **2016**, *55*, 5727–5732. [\[CrossRef\]](#)
17. Barandun, G.; Soprani, M.; Naficy, S.; Grell, M.; Kasimatis, M.; Chiu, K.L.; Ponzoni, A.; Güder, F. Cellulose Fibers Enable Near-Zero-Cost Electrical Sensing of Water-Soluble Gases. *ACS Sens.* **2019**, *4*, 1662–1669. [\[CrossRef\]](#)
18. Di Natale, C.; Macagnano, A.; Martinelli, E.; Paolesse, R.; D'Arcangelo, G.; Roscioni, C.; Finazzi-Agrò, A.; D'Amico, A. Lung cancer identification by the analysis of breath by means of an array of non-selective gas sensors. *Biosens. Bioelectron.* **2003**, *18*, 1209–1218. [\[CrossRef\]](#)
19. Mougang, Y.K.; Di Zazzo, L.; Minieri, M.; Capuano, R.; Catini, A.; Legramante, J.M.; Paolesse, R.; Bernardini, S.; Di Natale, C. Sensor array and gas chromatographic detection of the blood serum volatolomic signature of COVID-19. *iScience* **2021**, *24*, 102851. [\[CrossRef\]](#) [\[PubMed\]](#)
20. Kirchmeyer, S.; Reuter, K. Scientific importance, properties and growing applications of poly(3,4-ethylenedioxythiophene). *J. Mater. Chem.* **2005**, *15*, 2077–2088. [\[CrossRef\]](#)
21. Bai, H.; Shi, G. Gas Sensors Based on Conducting Polymers. *Sensors* **2007**, *7*, 267–307. [\[CrossRef\]](#)
22. Velasco-Bosom, S.; Karam, N.; Carnicer-Lombarte, A.; Gurke, J.; Casado, N.; Tomé, L.C.; Mecerreyes, D.; Malliaras, G.G. Conducting Polymer-Ionic Liquid Electrode Arrays for High-Density Surface Electromyography. *Adv. Health Mater.* **2021**, *10*, 2100374. [\[CrossRef\]](#) [\[PubMed\]](#)
23. Hamachi, T.; Nishimura, K.; Kouno, H.; Kawashima, Y.; Tateishi, K.; Uesaka, T.; Kimizuka, N.; Yanai, N. Porphyrins as Versatile, Aggregation-Tolerant, and Biocompatible Polarizing Agents for Triplet Dynamic Nuclear Polarization of Biomolecules. *J. Phys. Chem. Lett.* **2021**, *12*, 2645–2650. [\[CrossRef\]](#)
24. Manzini, I.; Schild, D.; Di Natale, C. Principles of odor coding in vertebrates and artificial chemosensory systems. *Physiol. Rev.* **2022**, *102*, 61–154. [\[CrossRef\]](#)
25. Dini, F.; Martinelli, E.; Pomarico, G.; Paolesse, R.; Monti, D.; Filippini, D.; D'Amico, A.; Lundström, I.; Di Natale, C. Chemical sensitivity of self-assembled porphyrin nano-aggregates. *Nanotechnology* **2009**, *20*, 55502. [\[CrossRef\]](#)

26. Magna, G.; Sivalingam, Y.; Martinelli, E.; Pomarico, G.; Basoli, F.; Paolesse, R.; Di Natale, C. The influence of film morphology and illumination conditions on the sensitivity of porphyrins-coated ZnO nanorods. *Anal. Chim. Acta* **2014**, *810*, 86–93. [[CrossRef](#)]
27. Araque, J.S.A.; Gonçalves, J.M.; Nakamura, M.; Rossini, P.; Angnes, L.; Araki, K.; Toma, H.E. GO composite encompassing a tetraruthenated cobalt porphyrin-Ni coordination polymer and its behavior as isoniazid BIA sensor. *Electrochimica Acta* **2019**, *300*, 113–122. [[CrossRef](#)]
28. Avossa, J.; Paolesse, R.; Di Natale, C.; Zampetti, E.; Bertoni, G.; De Cesare, F.; Scarascia-Mugnozza, G.; Macagnano, A. Electro-spinning of Polystyrene/Polyhydroxybutyrate Nanofibers Doped with Porphyrin and Graphene for Chemiresistor Gas Sensors. *Nanomaterials* **2019**, *9*, 280. [[CrossRef](#)] [[PubMed](#)]
29. Dini, F.; Magna, G.; Martinelli, E.; Pomarico, G.; Di Natale, C.; Paolesse, R.; Lundström, I. Combining porphyrins and pH indicators for analyte detection. *Anal. Bioanal. Chem.* **2015**, *407*, 3975–3984. [[CrossRef](#)]
30. D'Amico, A.; Di Natale, C. A contribution on some basic definitions of sensors properties. *IEEE Sens. J.* **2001**, *1*, 183–190. [[CrossRef](#)]
31. Cristaldi, D.A.; Capuano, R.; D'Urso, A.; Randazzo, R.; Paolesse, R.; Di Natale, C.; Purrello, R.; Fragalà, M.E.; D'Urso, A.; Razzo, R. Spontaneous Deposition of Porphyrin-Based Layers on Polylysinated Substrates: Role of the Central Metal on Layer Structural and Sensing Properties. *J. Phys. Chem. C* **2015**, *120*, 724–730. [[CrossRef](#)]
32. Magna, G.; Muduganti, M.; Stefanelli, M.; Sivalingam, Y.; Zurlo, F.; Di Bartolomeo, E.; Catini, A.; Martinelli, E.; Paolesse, R.; Di Natale, C. Light-Activated Porphyrinoid-Capped Nanoparticles for Gas Sensing. *ACS Appl. Nano Mater.* **2021**, *4*, 414–424. [[CrossRef](#)]
33. Murthy, R.; Pavlidis, I. Noncontact measurement of breathing function. *IEEE Eng. Med. Biol. Mag.* **2006**, *25*, 57–67. [[CrossRef](#)] [[PubMed](#)]